Available online at www.sciencedirect.com
SCIENCE DIRECT
Polymer 46 (2005) 8034–8044
polymer
www.elsevier.com/locate/polymer

Spatially resolved studies on the photopolymerization of dimethacrylate monomers

S.G. Pereira, N. Reis, T.G. Nunes*

Departamento de Engenharia de Materiais/IST e ICEMS/IST, Av. Rovisco Pais 1, 1049-001 Lisboa, Portugal

Received 7 December 2004; received in revised form 13 April 2005; accepted 9 June 2005
Available online 27 July 2005

Abstract

The photopolymerization of four dimethacrylate monomers under different irradiating conditions was followed in situ by ^{1}H stray-field magnetic resonance imaging (^{1}H STRAFI-MRI). This technique is capable of discriminating local changes at a spatial resolution of tens of micron and is suitable for studying larger samples than infrared spectroscopy and photocalorimetry. The evolution of proton magnetization with irradiation time and intensity was recorded and correlated with volumetric polymerization shrinkage, extent of reaction and spatially resolved reaction rates.

Keywords: Dimethacrylates; Photopolymerization; Kinetics

1. Introduction

Photopolymerization of multifunctional monomers or oligomers, often referred to as radiation curing, is a ubiquitous technology in specialty polymer processing [1,2]. Key and competitive advantages arise from the possibility of spatially controlling the polymerization by selectively irradiating the desired regions and the ultra-fast reaction rates achievable under intense radiation [3]. Additionally, it is a solvent-free (or solvent-poor) and energy efficient technology as polymerizations can be conducted at room temperature, and thus considered economical with minimum environmental impact.

Common applications of this technology include a wide variety of coatings, paints, printing inks, adhesives, composite materials and dental restorations. Most of these applications are two-dimensional in their essence, i.e. only thin layers (typically 100 μm or less) are polymerized at a time. There are cases, however, where polymerization is desirable to occur in thicker layers or bulk specimens. A paradigmatic example is the photopolymerization of resins and composites commonly used in dental restorations. In fact, several of the established photopolymerization processes adopt thin-layer approaches given the difficulties associated with light attenuation through 'optically thick' films. In these situations, the radiation absorbing species in the formulations lead to light intensity gradients from the irradiated surface to the interior of the specimen and hence to non-uniform rates of polymerization. As a result, polymer network formation occurs in an inhomogeneous fashion with almost inevitable deleterious consequences to the product final properties. Therefore, understanding the bulk polymerization of photocurable formulations seems a worth undertaking.

Spatially resolved photopolymerization studies were already reported on resin based dental materials, which were performed using ^{1}H STRAFI-MRI [[4–7]]. Otherwise, previous work in this area has, to a great extent, been limited to theoretical predictions [8–11] due to experimental difficulties associated with spatially resolved measurements of polymerization. Despite their usefulness in describing the mechanisms, most of these models rely on idealized conditions and assumptions to integrate the constitutive differential equations, such as quasi-static phenomena with physical and thermal properties constant throughout the reaction, absence of volume shrinkage, monochromatic light sources, and idealized boundary conditions. Moreover, they rely on the extrapolation of experimental data obtained for thin films (mostly by differential photocalorimetry and

* Corresponding author. Tel.: +351 21 81418103; fax: +351 21 8418101.
E-mail address: teresa.nunes@ist.utl.pt (T.G. Nunes).

0032-3861/$ - see front matter © 2005 Elsevier Ltd. All rights reserved.
doi:10.1016/j.polymer.2005.06.086

infrared spectroscopy) to predict bulk phenomena. Nevertheless, a valuable detailed investigation of the bulk photopolymerization kinetics of 1 mm thick layers of triethylene glycol dimethacrylate (TEGDMA) was performed as a function of various parameters such as photosensitizer/reducing agent concentrations, temperature, presence of air/N_2 [12]. So far, a comparative spatially resolved study was not carried out on the photopolymerization of dimethacrylate monomers. Here, we present the results of ^{1}H STRAFI-MRI combined with in situ irradiation as means to investigate the influence of structural parameters on the process kinetics of TEGDMA and three bis-GMA (2,2-bis[4-(2-hydroxy-3-methacryloxyprop-1-oxy) phenyl] propane) analogues. These are potentially good candidates, for example, to replace TEGDMA, a conventional used diluent, in bis-GMA polymeric dental matrices. The influence of these new diluent agents, diluent ratio and filler content on relevant mechanical properties of several novel composite resins containing bis-GMA as resin matrices and the comparison with the properties of composites based on TEGDMA were recently reported [13].

2. Experimental section

2.1. Materials

In the present study the photopolymerization behavior of four di-functional methacrylate monomers was investigated: TEGDMA and three dimethacrylate monomers of propoxylated diphenols. TEGDMA was used as received (Aldrich Chemical Co., Milwaukee, WI, USA) and the following three bis-GMA analogues were synthesized, purified and stored according to the earlier described method [14,15]: 2,2-bis[4-(2-methacryloxyprop-1-oxy) phenyl] propane, CH_3 bis-GMA, 1,1,1,3,3,3-hexafluoro-2,2-bis[4-(2-methacryloxyprop-1-oxy) phenyl] propane, CF_3 bis-GMA, and 2,2-bis[4-(2-methacryloxyethyl-1-oxy) phenyl] propane, CH bis-GMA (Fig. 1). An inhibitor (hydroquinone, 1 mol%) was added to the starting materials. Camphorquinone (CQ, Aldrich Chemical Co., Milwaukee, WI, USA) (1 mol%) and *N*,*N*,dimethyl-*p*-toluidine (DMPT, Aldrich Chemical Co., Milwaukee, WI, USA) (1 mol%) were added to the different samples, as a photosensitizer and a reducing agent initiator, respectively, necessary to induce the photopolymerization. CQ was sublimed at 140 °C under reduced pressure before using and DMPT was used as received. CQ is a widely used free radical photoinitiator in dental resin formulations, with one of the absorption bands ranging from 350 to 525 nm with a maximum at 468 nm, hence suitable for visible (blue) light polymerization. Table 1 shows concentration of double bonds, glass transition and viscosity of the four dimethacrylate monomers investigated.

2.2. Methods

One-dimensional ^{1}H STRAFI images, projections along an axis, were acquired from the liquid and from the photopolymerized monomers using a Bruker MSL 300P spectrometer, under the static magnetic field gradient of 37.5 T m^{-1} generated near the edges of the 89 mm superconducting coil. A dedicated Bruker STRAFI probe-head was tuned to 123.4 MHz, which gives ^{1}H and ^{19}F resonances at 2.9 and 3.1 T, respectively; these field strengths were obtained just outside the bore of the magnet. The spatial separation of the two resonances was 4.9 mm. Since only thin slices are observed at a time, 1D imaging of bulk specimens was conducted by moving the sample linearly in the direction of the field gradient to ensure that the volume under analysis experiences the same field conditions. Each liquid sample was introduced in a cylindrical glass vial (12 mm height and 8 mm inner diameter) filled up to 7–10 mm height and placed in the probe-head, in order to be irradiated in situ over cumulative irradiation periods until a total exposure time of 400 s. The irradiation was conducted by means of a custom-made optical fibre cable connected to a conventional quartz–tungsten–halogen light curing unit (Optilux 401, Demetron Research Corp., Danbury, CT, USA) and guided to the top of the probe-head radio frequency coil. This light source is polychromatic emitting in the range of 385–525 nm, with a maximum spectral irradiance at about 490 nm, hence suitable for CQ photoinitiation.

Two sets of samples for each formulation were prepared in order to be irradiated at two different light intensities: 1 or 25 mW cm^{-2}. One-dimensional images (profiles) were acquired along the container axis after each irradiation period. A reference signal for the intensities was obtained from a disc about 0.5 mm thick, made of commercial plastic or PMMA, which was placed under the glass vials. The photopolymerization was carried out at room temperature (about 22 °C). The magnetization was recorded as multiple 8 spin-echo trains. Each echo train was generated by the RF pulse sequence 90°_x-τ-[90°_y-τ-echo-τ]$_8$, where $90^\circ_{x,y}$ represents a 90° pulse of relative phase x or y and τ is a short time delay; the RF pulse duration (t_p) and echo time (TE) were 10 and 35 μs, respectively, (see [6] for details). Each data slice in the STRAFI-MRI profiles is the result of the summation of the eight echoes. In STRAFI-MRI, the linear resolution Δx can be estimated by $\sqrt{3}\pi/(t_p\gamma_H G_z)$, with t_p the RF pulse duration that is related to the frequency range to be excited, γ_H the proton gyromagnetic ratio (267.5 Mrad T^{-1}) and G_z the magnetic field gradient along the Z axis, also the axis of the static magnetic field [17], providing a figure of about 60 μm for the excited slice thickness.

Spatially resolved kinetic data (extension of reaction and reaction rate) were derived from changes observed in proton magnetization intensity as a function of irradiation time for each slice. The final volumetric polymerization shrinkage (in %) was determined for all monomers and irradiating

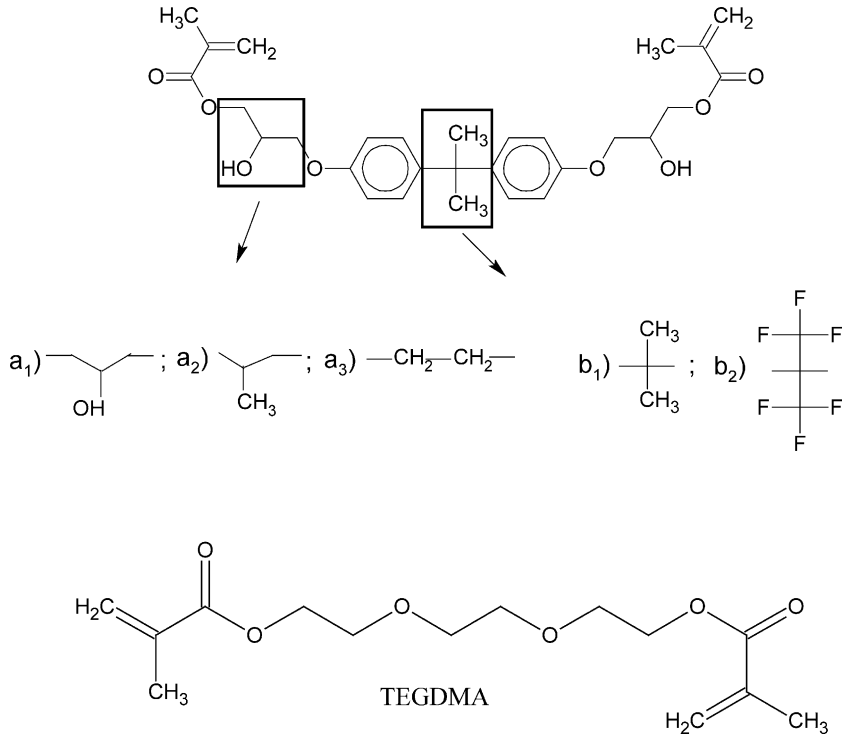

Fig. 1. Structural modification of bis-GMA (a_1;b_1) in terms of core and side chain replacements: CH_3 bis-GMA (a_2;b_1), CF_3 bis-GMA (a_2;b_2), CH bis-GMA (a_3; b_1) and TEGDMA structure.

conditions employed, according to a method previously described [7,18], as: [Σ(magnetization of each slice of the monomer, MM) − Σ(magnetization of each slice of the homopolymer obtained after 400 s cumulative irradiation time, MP) × 100]/Σ(MM). The highest intensity of MP was used as a reference for the intensity normalization of the magnetization MM and MP slices; Fig. 2 shows MM and MP data, preceding the normalization step. Seemingly, the extension of the photopolymerization (E_p) was obtained (in %) integrating the profiles prior (slices MM) and subsequent to exposure (slices MPn), as: [Σ(MM − MPn) × 100]/ Σ(MM). The normalization of MM and MPn was based on the assignment of 1 arb. unit to the highest magnetization intensity obtained from the reference signal; MM and MPn data (in arb. units) may be directly obtained from Fig. 2.

Post-cure images (typically after 24 h) were also obtained for all samples. In order to assess the final degree of double bond conversion and establish comparisons with the extend of the curing reaction obtained using ^{1}H STRAFI-MRI, post-cured samples were prepared and analyzed by infrared (FTIR) spectroscopy according to widely accepted procedures [19].

3. Results

In order to obtain the spatially resolved kinetics for the curing of the monomers, magnetization profiles were acquired prior irradiation and after the cumulative irradiation periods of 4, 8, 16, 24, 44, 100, 150, 200, 250, 300, 350, 400 s. The profiles acquired after periods of 24 h, following the total irradiation time, provided preliminary information on the monomer post-curing evolution. Typical STRAFI-MRI profiles recorded during the curing reactions of the four monomers at various conditions of irradiation time and light intensity are shown in Fig. 2(A)–(D), representing the evolution of ^{1}H magnetization profiles with accumulated irradiation time; it must be noticed that, in

Table 1
Glass transition, viscosity and volumetric polymerization shrinkage (VPS, %) obtained after a total, cumulative, irradiating period of 400 s (first value) at the indicated light-intensity and following a post-cure period of 24 h (second value)

Monomer	Concentration of double bonds (mol kg^{-1})	T_g (°C)	Viscosity [13] (Pa s)	VPS (%)	
				1 mW cm^{-2}	25 mW cm^{-2}
TEGDMA	6.99	−81.7 [16]	0.015	4.80–6.52	6.81–7.24
CH_3 bis-GMA	4.16	−24.0 [7]	8.4	1.38–1.46	2.20–2.30
CF_3 bis-GMA	3.40	−20.4 [16]	39.1	0.85–0.90	1.17–2.04
CH bis-GMA	4.42	−24.0 [16]	55.2	0.91–0.92	2.00–2.20

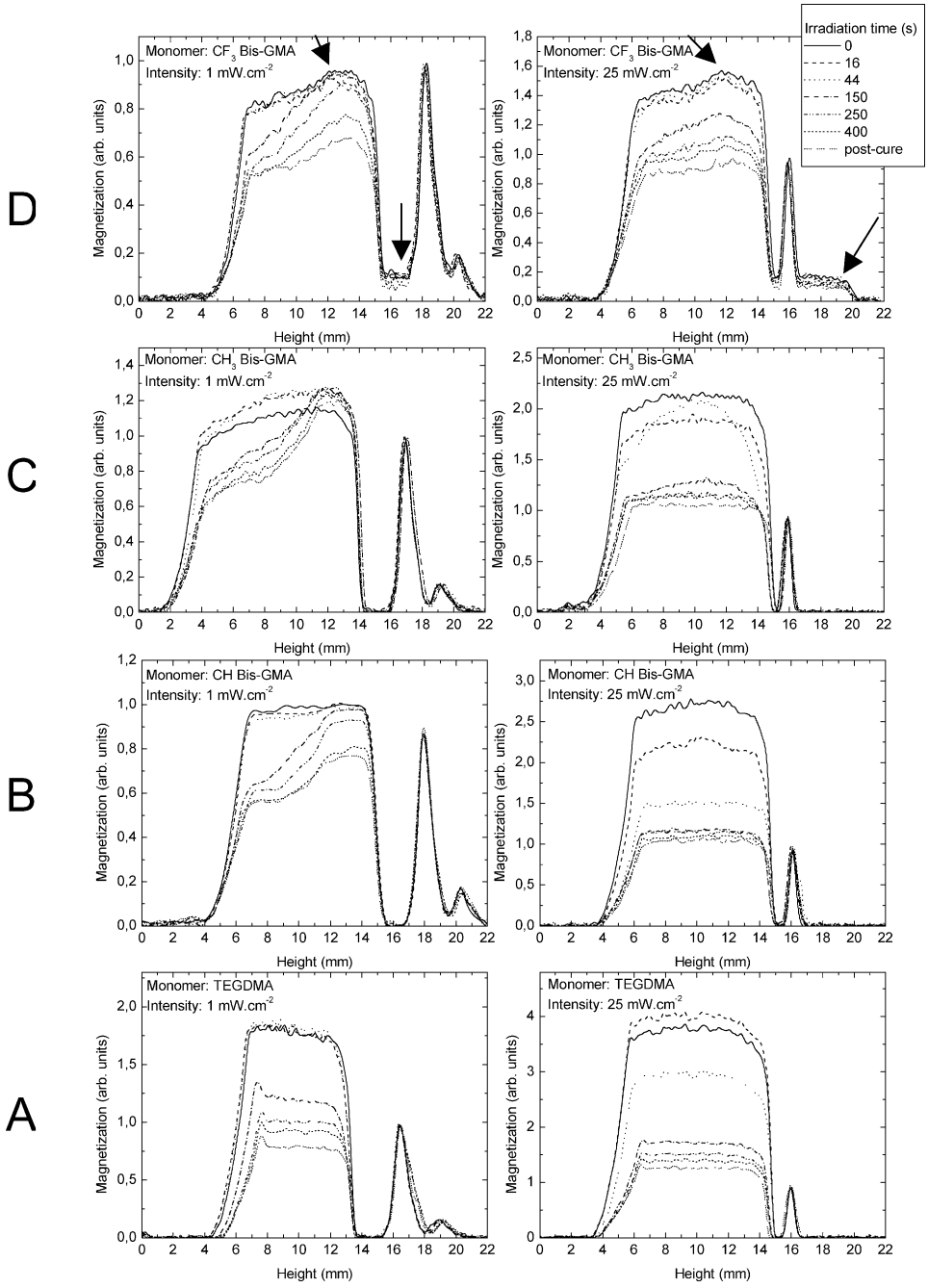

Fig. 2. ^{1}H magnetization profiles for various, cumulative, irradiation times (0, 16, 44, 150, 250 and 400 s) at the light intensities 1 and 25 mW cm^{-2}, respectively; post-cure profiles are also shown, which were recorded about 24 h after the last irradiation period. Monomers and irradiating intensities are labeled in the charts: (A) TEGDMA, (B) CH bis-GMA, (C) CH_3 bis-GMA and (D) CF_3 bis-GMA. The sharp signal shown on the right side of the profiles is either from a commercial plastic disk or from a PMMA disk, which were used as a reference for the magnetization intensities.

these figures, the profiles are rotated of 90° and, consequently, the sample surfaces and the reference signals obtained from plastic discs, are shown on the left- and on the right-side of the plots, respectively. The magnetization was normalized assigning 1 arb. unit to the reference signal.

The first general observations are the decrease in signal intensity and the narrowing of the profiles after exposure to light. The latter effect is clearly associated with contractions during polymerization and hence overall volume reduction. Because cured systems exhibit extensively lower magnetization, an estimate of the extent of the reaction, which must not be considered here as the degree of double bond conversion (DC), could be directly drawn from magnetization measurements. The decrease of magnetization intensity with exposure time is clearly associated to the loss of proton mobility with evolving polymerization, in spite of the fact that the proton density of each slice increases proportionally to the volume shrinkage, since the number of protons

remains constant during the curing reaction. Hence, the observed variations could be used to determine the polymerization shrinkage and E_p throughout the reaction. Table 1 summarizes the results obtained for the overall volumetric polymerization shrinkage (VPS) and Table 2 shows E_p values obtained by this method and DC figures obtained from FTIR spectroscopy measurements, in which case different regions were observed in order to minimize the errors due to the heterogeneity of the samples. Vitrification depends mainly on T_g and determines the degree of double-bond conversion; both follow the trend on VPS, measured using STRAFI:TEGDMA > CH_3 bis-GMA > CH bis-GMA > CF_3 bis-GMA.

Because the spatial separation of ^{1}H and ^{19}F resonances was shorter than the sample thickness (4.9 mm versus about 7–10 mm), the ^{19}F profiles of the CF_3 bis-GMA monomer were also recorded during the same experiment and are displayed, shifted 4.9 mm to the right-side of the corresponding ^{1}H profiles (Fig. 2(D)); profile regions where this effect may be clearly observed are indicated by arrows in Fig. 2(D). It is interesting to observe that, in comparison with ^{1}H data, ^{19}F signal intensity is much less affected by the ongoing curing reaction, as may be concluded from a close observation of profile regions containing only ^{19}F contribution; this is explained by the fact that CF_3 groups are located in the core part of the monomer and, consequently, are less influenced by mobility changes inherent to the curing reaction. Recently, ^{1}H and ^{19}F STRAFI-MRI profiles were used to follow the setting of a commercial glass-ionomer [20].

A closer examination of the profiles reveals that in some cases the magnetization increases slightly at the beginning of irradiation. This effect is seen for the lower viscosity monomers (TEGDMA and CH_3 bis-GMA) and is attributed to a dominant decrease in viscosity (hence increased molecular mobility) due to sample heating, over the decrease in mobility due to reaction at the early stages of polymerization. There are two sources of heat in the present experiments: That resulting from the light absorption (which is low at low exposure doses) and the heat released during polymerization, calculated to be 56 kJ mol^{-1} per methacrylate double bond [21].

The profiles shown in Fig. 2(A)–(D) also reveal the influence of light intensity on penetration depth. With exception of TEGDMA, all other monomers did not polymerize uniformly through the depth at 1 mW cm^{-2}. In particular, CH_3 bis-GMA profiles show that, for a layer near the bottom of the container and about 2 mm thick, the magnetization intensity remains very high and close to the value obtained for the liquid monomer, even after an irradiation time of 400 s; this observation indicates that unreacted monomer is the major species present in the mentioned region. Since the photoinitiator composition and concentration were fixed for all samples and irradiating conditions, the shape of a profile must depend on the physico–chemical properties of the monomer, which determine its reactivity; in particular, the viscosity and the glass transition of a monomer strongly influence the spatial distribution of free radicals, therefore, determining the initiation/propagation/termination reaction rates. Table 1 shows that TEGDMA has the lowest viscosity, of the order of 10^{-2} Pa s, and that the other three monomers have viscosities in the range 8–56 Pa s.

The increase of the irradiation intensity to 25 mW cm^{-2} (still about a factor of 20 less than the recommended value to be used by clinicians) lead to much more isotropic reactions and the depth of cure became higher than the sample thickness for all monomers.

The present experiments also reveal reaction inhibition near the surface exposed to air. This effect is commonly observed in monomers with high affinity for dissolving atmospheric oxygen, which is a well-known free radical scavenger, and was clearly observed for TEGDMA. Fig. 3 shows a contour plot of the magnetization signal intensity as a function of time and depth, where it can be observed that the system retains higher mobility near the top surface for longer periods of time. The effect is seen in a thickness of approximately 0.5 mm, remaining even after long post-cure

Table 2
Comparison between average extents of photopolymerization (E_p) obtained by STRAFI and maximum degree of conversion (DC) ranges obtained by FTIR that correspond to different regions of the cured, heterogeneous, resins

Monomer	Intensity (mW cm^{-2})		
	1	25	
	DC (%)	E_p (%)	DC (%)
TEGDMA	39/52	70.6	62/74
CH_3 bis-GMA	39/45	50.6	62/67
CF_3 bis-GMA	33/39	38.7	55/60
CH bis-GMA	37/42	59.9	58/62

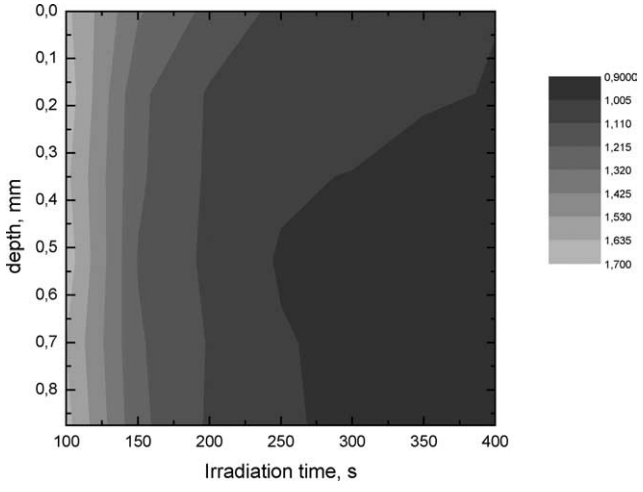

Fig. 3. Magnetization contour map of TEGDMA photopolymerization at 1 mW cm^{-2} as a function of exposure time and sample depth. Magnetization units are arbitrary but normalised to PMMA signal intensity.

periods being more pronounced at low exposure doses (Fig. 2(A)).

Neglecting the oxygen inhibitor effect, the following relationship can be used for the photopolymerization rate R_p of a thin monomeric film, under the assumption of a steady-state in radical species [9]:

$$R_p = \frac{K_p}{K_f^{1/2}}(2.3\phi_i\varepsilon_s I_0 C_s)^{1/2}[M_c] \quad (1)$$

K_p and K_f are the propagation and termination rate constants of the polymerization reaction, C_s concentration of the photosensitiser, $[M_c]$ is the monomer concentration, ϕ_i is the initiation quantum yield, ε_s is the molar absorptivity of the photosensitiser and I_0 is the light intensity at the exposed surface, which is constant for a thin film. For a sample about 10 mm thick, Eq. (1) is still valid but I_0 is no longer constant and for polychromatic radiation and after each cumulative irradiating period (t), the light intensity $I(x)$ follows the Lambert–Beer law, integrated over the wavelength [$\lambda 1$, $\lambda 2$] delimiting the photoinitiator efficient spectral range:

$$I(x,t) = C_s \int_{\lambda 1}^{\lambda 2} I_0(\lambda)\varepsilon_s(\lambda)\exp\left[-\sum_{i=1}^{N}\alpha_i(\lambda)\int_0^L C_i(x,t)\mathrm{d}x\right]\mathrm{d}\lambda \quad (2)$$

α_i the absorbance of the ith species (free monomer, oligomers and polymer network) and L the depth of cure. To a first approximation considering a single absorption at 468 nm for camphorquinone, which corresponds to the maximum peak, the variation of the light intensity with distance can be expressed as:

$$I(x,t) = C_s I_0(468)\varepsilon_s(468)\exp\left[-\sum_{i=1}^{N}\alpha_i(468)\int_0^L C_i(x,t)\mathrm{d}x\right] \quad (3)$$

The profiles obtained for the three bis-GMA analogues using a light intensity of 1 mW cm^{-2} (Fig. 2(A)–(D)) show spatial variation of the magnetization (M) with the distance (x) from the light source, which is more pronounced in the middle of the samples. The mono-exponential functions (4a) and (4b) were obtained by fitting the experimental data for CH_3 bis-GMA and CH bis-GMA at 1 mW cm^{-2}, respectively (Fig. 4):

$$M(x) = 0.01\exp\left(\frac{x}{3.1}\right) + 0.6 \quad (4a)$$

$$M(x) = 0.0003\exp\left(\frac{x}{1.7}\right) + 0.5 \quad (4b)$$

The functions (4a) and (4b) reproduce the variation of the light intensity with distance according to (3). At this stage, the need for the various parameters and their dependence in the above formulation make it impractical to conduct precise calculations for a more quantitative description.

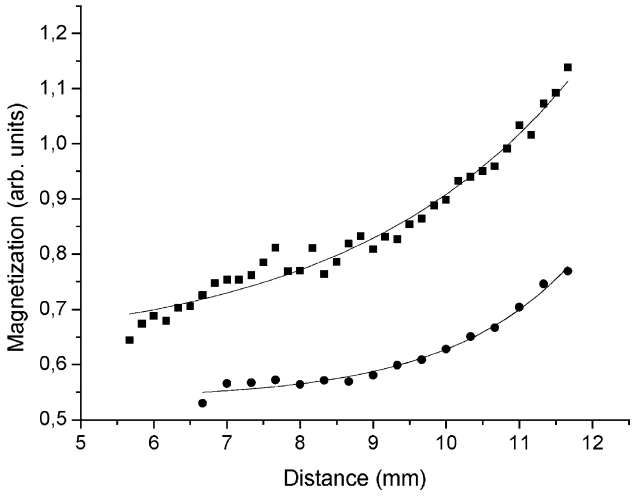

Fig. 4. ^{1}H magnetization (arb. units) of the monomers CH bis-GMA (●) and CH_3 bis-GMA (■), recorded after 400 s cumulative irradiation periods at a light intensity of 1 mW cm^{-2}, as a function of distance from the light source, which corresponds to sample height as shown in Fig. 2.

These issues will be further discussed in a forthcoming publication.

Using much longer echo trains (typically with 1024 echoes) than in the present study, it was earlier verified that the echo attenuation, in each long echo train, followed a double-exponential decay with the NMR acquisition time; the unreacted methacrylate group fraction was suggested to be represented by the relative amplitude of the component with longer exponential time constant decay, at the end of the irradiation period, enabling a so-called STRAFI degree of conversion (STRAFI-DC) to be defined [6]. In the present study, this acquisition mode was not used because it does not allow obtaining spatially resolved data; at present, due to hardware and software constraints, only single-slice data can be recorded.

Another approach to obtain information on the curing extent is tentatively proposed here, which is valid for much shorter echo trains and is based on the reasonable assumption that protons in unreacted methacrylate groups and monomers are considered to be the dominant contribution for the profiles obtained from the cured samples. Moreover, the magnetization ($M(x)$) is assumed here to be proportional to the summation of free monomer concentration [$M_c(x)$] and pendant unreacted methacrylate group concentration.

Thus, E_p was obtained integrating the profiles prior and subsequent to exposure. Table 2 shows the average conversion values obtained by STRAFI and those obtained by conventional FTIR analysis. Direct comparison can only be established when the samples are uniformly polymerized throughout the depth (i.e. all monomers at 25 mW cm^{-2} and TEGDMA at 1 mW cm^{-2}). Excellent agreement was found for both TEGDMA and CH bis-GMA, but the deviation found for the other two indicate that the results are dependent upon molecular structure. It must be noticed that

part of the ^{1}H profiles of CF_3 bis-GMA do not contain the magnetization contribution from the protonated methyl groups in the bisphenol moieties and this fact may explain the larger difference between FTIR and STRAFI-MRI data observed in Table 2, as compared with the other data.

Spatial discrimination of the reaction kinetics can be determined using the information obtained at different periods of irradiation. An example is shown in Fig. 5 for one of the monomers at two different irradiation intensities and identical exposure times. As expected, increasing irradiation intensity leads to faster rates of polymerization, and higher extension of the reaction. This is due to a combined effect of enhanced free radical production and higher temperatures achieved in the sample from increased heat of reaction (faster rates). In almost all cases, double bond conversion followed a sigmoidal type growth with exposure time, characteristic of multi-methacrylate polymerizations [e.g. [22]].

These systems are well known for exhibiting a period with no diffusional controls followed by an auto-acceleration region (dramatic increase in rate), during which only termination is diffusion-controlled; this period corresponds to the gelation-phase and is followed by a reaction–diffusion controlled termination region (with K_p constant) and an auto-deceleration region with reaction–diffusion controlled termination [23]. The latter is originated by reduced mobility in the system during polymer network formation, which generally leads to incomplete double bond conversion and higher rates of auto-acceleration than deceleration. As a consequence, an asymmetric sigmoidal growth is commonly observed for double bond conversion as a function of exposure time.

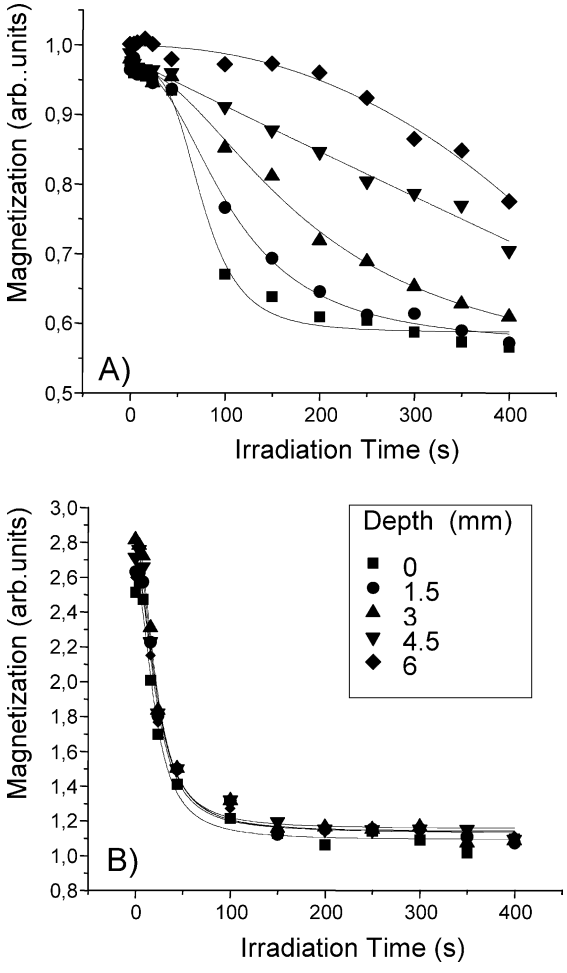

Fig. 5. ^{1}H magnetization (arb. units) as a function of irradiation time at various depths obtained for the monomer CH bis-GMA using two different irradiation intensities: (A) 1 mW cm^{-2} and (B) 25 mW cm^{-2}. The first slice of the profile obtained after 400 s cumulative irradiation time is the reference (0 mm) of the indicated depth values. The curves were obtained by fitting the experimental data with Eq. (6).

Recently, the degree of conversion of various photo-polymerized methacrylates determined by FTIR was expressed by means of a six fitting parameter equation consisting of the ratio between two 2nd order polynomials [22]. Here, to describe the extent of photopolymerization of each sample slice as a function of irradiation time, $E_p(t)$, we propose using a four fitting parameter sigmoidal equation of the form:

$$E_p(t) = 1 - \frac{M(t)}{M_i} \tag{5}$$

with

$$M(t) = \frac{M_i - M_f}{1 + \left(\frac{t}{t_h}\right)^p} + M_f \tag{6}$$

where $M(t)$ is the magnetization at time t, M_i is the magnetization recorded from the monomer, M_f is assigned to the end of the reaction (lower asymptote) and t_h the time at which half of the polymerization has occurred (i.e. t for $(M_i - M_f)/2$). The exponent p is an empirical constant reflecting the trend (positive for growth and negative for fall) and asymmetry shown by the $E_p(t)$ curve around its inflection point, and hence can be correlated to diffusion constraints. The fitting obtained with Eq. (6) for designated slices of one monomer can be seen in Fig. 5. It shall be noted that here $E_p(t)$ is different from the value assigned to DC because STRAFI magnetization profiles contain not only proton contributions from the polymer network but also from unreacted monomers and pendant methacrylate groups. Therefore, it is expected that the present determinations provide a lower bound to the actual DC.

The second derivative of Eq. (5) with respect to time shows that the parameter t_h is related to inflection point of the sigmoidal curve, corresponding to the maximum rate of polymerization R_{pmax} and t_{max}, by:

$$t_{max} = \left(\frac{p-1}{p+1}\right)^{1/p} t_h \tag{7}$$

For p values between 0 and 1 there is no inflection point in the curve, only a rate decrease corresponding to the vitrification phase. This behaviour is shown by CH_3 bis-GMA irradiated at 25 mW cm^{-2}; near the surface, gelation

has occurred in less than 4 s, which was the duration of the first irradiation period (Fig. 6). A similar shape of the rate curve was, for example, reported on bis-GMA and urethane dimethacrylate resin (UDMA) photopolymerizations followed by FT-IR spectroscopy [21] and, recently, on the photopolymerization of an adhesive containing UDMA in its formulation [18]. For p greater than 1, the inflection is introduced and the higher its value the better the approximation to a symmetric sigmoidal growth, i.e. less pronounced is the effect of diffusion constraints in the reaction and thus similar rates of autoacceleration and auto-deceleration. TEGDMA showed higher p values than the other monomers-particularly at 1 mW cm^{-2}-indicating a less pronounced effect of diffusion constraints due to the low viscosity and T_g (Table 1).

The reaction rate observed in a given slice as a function of time $R_p(t)$ can be directly obtained by differentiation as:

$$E'_p(t) = R_p(t) = \frac{(M_i - M_f)pt^{(p-1)}t_h^{-p}}{(1 + t^p t_h^{-p})^2 M_i} \quad (8)$$

As an illustration, Fig. 6 shows the plots of $E_p(t)$ and $R_p(t)$ at various depths obtained for one of the monomers revealing the characteristic asymmetry generally shown by these systems. Table 3, summarizes the overall results revealing opposite trends of the maximum reaction rate (R_{pmax}) and the time at which it occurs (t_{max}) with depth.

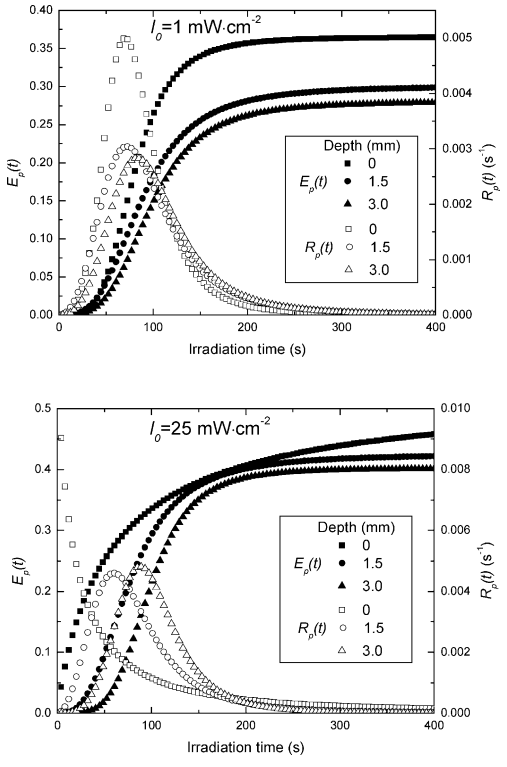

Fig. 6. Extent of photopolymerization and equivalent reaction rates determined by Eqs. (5) and (8), respectively, at various depths for the monomer CH_3 bis-GMA at 1 and 25 mW cm^{-2}.

Typically, the reaction becomes slower and its maximum rate occurs at longer irradiation periods with increasing depth; the effect being more pronounced for low exposure doses. For the photopolymerizations carried out at 25 mW cm^{-2} (more isotropic throughout the depth) R_{pmax} and t_{max} follow the trends shown in (a) and (b), respectively: (a) CH bis-GMA > TEGDMA > CH_3 bis-GMA > CF_3 bis-GMA; (b) CH bis-GMA < TEGDMA < CH_3 bis-GMA < CF_3 bis-GMA. These data demonstrates that CH bis-GMA is the monomer that most favors gelation, as the maximum photopolymerization rate was reached after the shortest irradiation time. Vitrification depends mainly on T_g and determines the degree of double bond conversion; both follow the trend on VPS, measured using STRAFI: TEGDMA > CH_3 bis-GMA > CH bis-GMA > CF_3 bis-GMA.

4. Discussion

In contrast to conventional imaging, the STRAFI-MRI technique exploits the fringe of the permanent magnetic field where a strong static magnetic field gradient is present. Using this gradient avoids the time required for generating (switching) the field gradients necessary for imaging, and hence the period between excitation and data acquisition can be of the order of few microseconds, that is, about 1000 times shorter than in conventional MRI. The STRAFI-MRI technique allows the observation of both solids (e.g. glassy polymers) and liquid components (e.g. monomers); the signal intensity depends on hydrogen concentration, but is also strongly affected by relaxation. This fact is not a disadvantage of the technique; on the other hand, it allows increasing contrast, which is then based on different molecular dynamics. The relaxation processes are mainly spin–spin and spin–lattice in the rotating frame relaxations, which are correlated with molecular mobility in the kHz range. They have time constants T_2 and $T_{1\rho}$, which are very short for rigid solids and longer for liquid components.

Each data slice in the STRAFI-MRI profiles (Fig. 2(A)–(D)) is the result of the summation of eight echoes, recorded over 280 μs, with echo-time 35 μs. Because the technique enables using such short echo times, the experiment approximates spin locking condition and this explains why the echo intensities decay away also according to $T_{1\rho}$. There were two main purposes for using trains of more than one echo: (a) To increase the signal/noise ratio by co-adding eight echoes and (b) to enhance the relaxation-weighting of the profiles, thus enabling better discrimination of liquid–gel–solid phase transitions. The first echo (obtained 35 μs after starting the experiment), which is only governed by spin–spin relaxation [24], refocus 100% and more than 90% of the magnetization from monomers (mobile, liquids) and cured resins (rigid, mostly solids), respectively. Different

Table 3
Results obtained for polymerization kinetics of the various monomers at different depths and irradiation intensities

Depth (mm)	Monomer							
	CF_3 bis-GMA				CH_3 bis-GMA			
	Intensity (mW cm^{-2})				Intensity (mW cm^{-2})			
	1		25		1		25	
	R_{pmax} (s^{-1})	t_{max} (s)	R_{pmax} (s^{-1})	t_{max} (s)	R_{pmax} (s^{-1})	t_{max} (s)	R_{pmax} (s^{-1})	t_{max} (s)
0	0.002	72	0.003	70	0.005	70	No. max	No. max
1.5	0.002	87	0.002	110	0.003	72	0.005	56
3	0.001	187	0.002	140	0.003	83	0.005	88
4.5	0.001	277	0.002	128	0.002	96	0.005	97
6	0.001	412	0.002	116	–	–	0.005	95
Depth (mm)	Monomer							
	CH bis-GMA				TEGDMA			
	Intensity (mW cm^{-2})				Intensity (mW cm^{-2})			
	1		25		1		25	
	R_{pmax} (s^{-1})	t_{max} (s)	R_{pmax} (s^{-1})	t_{max} (s)	R_{pmax} (s^{-1})	t_{max} (s)	R_{pmax} (s^{-1})	t_{max} (s)
0	0.005	66	0.018	12	0.004	121	0.008	40
1.5	0.003	70	0.016	14	0.006	120	0.009	42
3	0.002	100	0.018	14	0.005	117	0.008	41
4.5	–	–	0.018	13	0.004	113	0.009	42
6	–	–	0.017	14	–	–	0.008	39

The first slice of the profile obtained after 400 s cumulative irradiation time is the reference (0 mm) of the indicated depth values.

echoes have different contributions from T_2, $T_{1\rho}$ and T_1, which do not depend on the material under observation but on the magnetization coherence pathways that are generated by the RF pulse sequence applied under the permanent static magnetic field gradient G_z [24]. Moreover, it is known that while T_2 and $T_{1\rho}$ are both of the order of milliseconds for monomers, solid polymers exhibit T_2 on the microsecond timescale and 10 ms is a typically $T_{1\rho}$ value; T_1 is, in general, of the order of seconds. Therefore, it is mainly the shortening of T_2 throughout the curing reaction that induces a decrease of the profile intensity, hence enabling the reaction kinetics to be studied.

In the present study, because the photopolymerization reactions occurred without significant evaporation of any of the starting components, the decrease of ^1H magnetization with irradiation time was correlated with the extent of the curing reaction. This enabled to obtain spatially resolved photopolymerization kinetic data, which was acquired at room temperature and in the presence of oxygen from the atmosphere. During the early stages of the irradiation period, the viscosity of the monomer solution is governed by two competing mechanisms: (a) The increase in temperature, which will reduce the viscosity and (b) the polymer's increasing molecular weight, which will increase viscosity. As the curing progresses, the viscosity increases and the material becomes more rigid; it is then expected that the average ^1H T_2 decreases, thereby leading to less intense recorded magnetization. The spatial dependence of the signal intensity is thus correlated with the volumetric distribution of less mobile domains.

Hence, the evolution of curing was locally monitored by the changes observed to the ^1H magnetization signal intensity, which depend on hydrogen concentration but are strongly weighted essentially by spin–spin and spin–lattice in the rotating frame relaxations, that is, by the proton mobility in the kHz frequency range [4,6]. Accordingly, intensity variations can be directly related to volumetric contractions and extent of reaction.

Most of the composite resins widely used in restorative dentistry contain the highly viscous monomer bis-GMA and low viscosity monomers, used as diluents, in order to achieve high filler loading. TEGDMA, in particular, has been extensively used for such purpose. When the effect of dilution with TEGDMA on the kinetics of bis-GMA polymerization and on DC has been evaluated using DSC and ^{13}C NMR spectroscopy, systems with lower viscosity and lower glass transition temperature (T_g) exhibited higher DC and a high correlation was obtained between T_g of the monomer mixture and DC [25].

Monomers with shorter molecular length (with identical functionality, hence with a high concentration of double bonds) are expected to react faster; in addition, monomers of higher flexibility (lower T_g) and lower viscosity are expected to reach a higher degree of conversion even if the polymerization is carried out at ambient temperature.

The results obtained when using a very low intensity of light (1 mW cm^{-2}) could be explained on the basis that, with exception of TEGDMA, all other monomers alone could show some absorption within the spectral band width of the light source. According to Eqs. (1) and (3) this would lead to higher levels of attenuation with depth and consequently decreased rates of initiation. UV–Visible spectrophotometric measurements did not confirm this hypothesis, since the four monomers showed very low absorption within the spectral range of interest. On the other hand, partial polymerization of the synthesized monomers and the corresponding viscosity increase, in conjunction with I_0 too low, could also account for the observed profile STRAFI-MRI differences. A detailed observation of the profiles obtained from the liquids (first plot on the left-side of Fig. 2(A)–(D)) confirmed the latter assumption: While the profile and the reference signal show similar magnetization for each of the three synthesized monomers, the profile obtained from TEGDMA is about two times more intense, thus reflecting a corresponding slower spin echo decay, since each data point in the profile is obtained as the summation of the echo intensities in each echo train, as it was already pointed out. The presence of oligomers in the synthesized monomer solutions may be due to a lower concentration of the stabilizer (hydroquinone) being added, as compared with commercial TEGDMA. Up to 1.5 mm depth, the time to reach the maximum rate (t_{max}) is within the range 66–87 s for the three bis-GMA analogues while for TEGDMA t_{max} reaches 120 s; these data are in agreement with a narrower window for these monomers to start vitrification, as compared with TEGDMA, effect which is enhanced by the more important inhibition role of oxygen in this monomer.

The four independent parameter sigmoidal model proposed to describe the time dependence of the photopolymerization extent, revealed suitable to fit our experimental data. Moreover, the fitting parameters can be associated to reaction phenomena, such as the correlation of the exponent p and reaction–diffusion constraints. It should be noted that Eq. (6) is also suitable to describe the evolution of double bond conversion with time determined by FTIR spectroscopy. In this case the number of fitting parameters is reduced to three as the initial value is zero. Fitting Eq. (6) to the data provided in [21] results in better correlation factors (r^2) than those reported for a six parameter fitting model, in almost all cases.

Recently, relevant mechanical properties of bis-GMA/TEGDMA, bis-GMA/CH_3 bis-GMA and bis-GMA/CF_3 bis-GMA composite resins were evaluated as a function of filler loading and polymeric matrix composition [13]. Materials with CH_3 bis-GMA showed an enhanced microhardness while flexural strength was higher for matrices containing TEGDMA. Overall, results were well correlate with an increase in the extent of polymerization due to the higher flexibility of the less viscous comonomer starting system and the hydrophobic character of the bis-GMA analogues.

5. Conclusions

Spatial discrimination allowed following the cure behavior of thick films under ambient conditions, which are seldomly reported in the open literature due to experimental difficulties and complex to model non-linear behavior. Semi-quantitative description of the photopolymerization behavior could be obtained by monitoring proton mobility evolution with light-curing time using STRAFI-MRI. Determination of pseudo-reaction parameters such as extent of reaction and cure rate were provided.

Although the present investigations were restricted to the photopolymerization of dimethacrylate monomers relevant to dental applications, the same methodology can be extended to other multifunctional monomer systems. A key feature of the technique is the analysis of samples showing non-uniform polymerization. This effect is difficult or impossible to spatially resolve by FTIR or photocalorimetry due to experimental constraints, but can be directly evaluated by STRAFI-MRI.

Acknowledgements

This work was supported by the Portuguese Foundation for Science and Technology (Project POCTI/33193/99 and grants PRAXIS/BD/20066/99 and BPD/7112/2001 acknowledged by SGP and NR, respectively).

References

[1] Pappas SP. Radiation curing: Science and technology. Topics in applied chemistry. New York: Plenum Press; 1992.
[2] Fouassier JP, Rabek JF. Radiation curing in polymer science and technology. London: Elsevier Applied Science; 1993.
[3] Decker C. Prog Polym Sci 1996;21(4):593–650.
[4] Nunes TG, Pires R, Perdigão J, Amorim A, Polido M. Polymer 2001; 42:8051–4.
[5] Lloyd CH, Scrimgeour SN, Lane DM, Hunter G, McDonald PJ. Dent Mater 2001;17(5):381–7.
[6] Nunes TG, Guillot G, Pereira SG, Pires R. J Phys D, Appl Phys 2002; 35(11):1251–7.
[7] Pereira SG, Nunes TG, Kalachandra S. Biomaterials 2002;23(18): 3799–806.
[8] Pananakis D, Watts DC. J Mater Sci 2000;35(18):4589–600.
[9] Lecamp L, Lebaudy P, Youssef B, Bunel C. Polymer 2001;42(21): 8541–7.
[10] Terrones G, Pearlstein AJ. Macromolecules 2001;34(26): 8894–906.
[11] Goodner MD, Bowman CN. Chem Eng Sci 2002;57(5):887–900.
[12] Nie J, Linden LA, Rabek JF, Fouassier JP, Morlet-Savary F, Scigalski F, et al. Acta Polym 1998;49(4):145–61.
[13] Pereira SG, Osorio R, Toledano M, Nunes TG. Dent Mater; in press.
[14] Kalachandra S, Taylor DF, Deporter CD, Grubbs HJ, McGrath JE. Polymer 1993;34(4):778–82.
[15] Sankarapandian M, Shobha HK, Kalachandra S, McGrath JE, Taylor DF. J Mater Sci, Mater Med 1997;8(8):465–8.
[16] Pereira SG, Stephen MG. Private communication.
[17] McDonald PJ. Prog Nucl Magn Reson Spectrosc 1997;30:69–99.

[18] Nunes TG, Ceballos L, Osorio R, Toledano M. Biomaterials 2005; 26(14):1809–17.
[19] Rueggeberg FA, Hashinger DT, Fairhurst CW. Dent Mater 1990;6(4): 241–9.
[20] Pires R, Nunes TG, Abrahams I, Hawkes GE, Morais C, Fernandez C. J Mater Sci: Mater Med 2004;15(3):201–8.
[21] Jakubiak J, Sionkowska A, Linden LA, Rabek JF. J Therm Anal Calorim 2001;65(2):435–43.
[22] Sideridou I, Tserki V, Papanastasiou G. Biomaterials 2002;23(8): 1819–29.
[23] Goodner MD, Lee HR, Bowman CN. Ind Eng Chem Res 1997;36: 1247–52.
[24] Bain AD, Randall EW. J Magn Res Ser A 1996;123:49–55.
[25] Morgan DR, Kalachandra S, Shobha HK, Gunduz N, Stejskal EO. Biomaterials 2000;21:1897–903.